Biomaterials 34 (2013) 9341–9351

Contents lists available at ScienceDirect

Biomaterials

journal homepage: www.elsevier.com/locate/biomaterials

Functional ultrasound imaging for assessment of extracellular matrix scaffolds used for liver organoid formation

Ryan C. Gessner [a], Ariel D. Hanson [a,b,1], Steven Feingold [a,1], Avery T. Cashion [a], Ana Corcimaru [b], Bryant T. Wu [a,b], Christopher R. Mullins [e], Stephen R. Aylward [e], Lola M. Reid [b,c,d,**,2], Paul A. Dayton [a,d,*,2]

[a] UNC/NCSU Joint Department of Biomedical Engineering, UNC School of Medicine, Chapel Hill, NC 27599, USA
[b] Department of Cell Biology and Physiology, UNC School of Medicine, Chapel Hill, NC 27599, USA
[c] Program in Molecular Biology and Biotechnology, UNC School of Medicine, Chapel Hill, NC 27599, USA
[d] Lineberger Cancer Center, UNC School of Medicine, Chapel Hill, NC 27599, USA
[e] Kitware, Inc., 101 East Weaver St, Carrboro, NC 27510, USA

ARTICLE INFO

Article history:
Received 13 July 2013
Accepted 10 August 2013
Available online 4 September 2013

Keywords:
Acoustic angiography
Microbubble
Extracellular matrix
Scaffolds
Liver
Organoids

ABSTRACT

A method of 3D functional ultrasound imaging has been developed to enable non-destructive assessment of extracellular matrix scaffolds that have been prepared by decellularization protocols and are intended for recellularization to create organoids. A major challenge in organ decellularization is retaining patent micro-vascular structures crucial for nutrient access and functionality of organoids. The imaging method described here provides statistical distributions of flow rates throughout the tissue volumes, 3D vessel network architecture visualization, characterization of microvessel volumes and sizes, and delineation of matrix from vascular circuits. The imaging protocol was tested on matrix scaffolds that are tissue-specific, but not species-specific, matrix extracts, prepared by a process that preserved >98% of the collagens, collagen-associated matrix components, and matrix-bound growth factors and cytokines. Image-derived data are discussed with respect to assessment of scaffolds followed by proof-of-concept studies in organoid establishment using Hep3B, a human hepatoblast-like cell line. Histology showed that the cells attached to scaffolds with patent vasculature within minutes, achieved engraftment at near 100%, expressed liver-specific functions within 24 h, and yielded evidence of proliferation and increasing differentiation of cells throughout the two weeks of culture studies. This imaging method should prove valuable in analyses of such matrix scaffolds.

1. Introduction

Liver transplantation is the primary treatment for end-stage liver disease [1]. Currently, more than 16,000 adults and children are in need of liver transplants. Unfortunately, the number of livers available for transplantation are in short supply [2]. An alternative to organ transplantation is to support patients using an extracorporeal liver-assist device (LAD). A LAD is a bioreactor comprised of liver cells harvested from donor livers and incorporated into a network of hollow dialysis fibers that mimic blood vessels, which can connect to the patient and thus serve as a bioartificial liver [3,4]. Such bioartificial liver devices provide temporary relief for one to two weeks or until an organ is available for transplantation. They cannot be used longer, since liver cells seeded into all extant forms of bioreactors attach and deposit extracellular matrix and other cellular components onto the hollow fibers, causing “fouling” or clogging of the fibers’ pores, limiting the life span of the device [5].

A more robust alternative is to develop human liver organoids that can be incorporated into a LAD to enable hemodialysis; this provides a more stable and fully functional bioartificial liver in which vascular channels are provided by the native extracellular

* Corresponding author. UNC/NCSU Joint Department of Biomedical Engineering, Lineberger Cancer Center, Chapel Hill, NC 27599-6136, USA.
** Corresponding author. Department of Cell Biology and Physiology, Program in Molecular Biology and Biotechnology, Lineberger Cancer Center, Chapel Hill, NC 27599-7038, USA.
E-mail addresses: gessner.ryan@gmail.com (R.C. Gessner), adhanson@email.unc.edu (A.D. Hanson), sgfeingold@gmail.com (S. Feingold), zackcashion@gmail.com (A.T. Cashion), acorcimaru@gmail.com (A. Corcimaru), btwu10@gmail.com (B.T. Wu), christopher.mullins@kitware.com (C.R. Mullins), stephen.aylward@kitware.com (S.R. Aylward), Lola.M.Reid@gmail.com (L.M. Reid), padayton@bme.unc.edu (P.A. Dayton).
[1] Co-equal second authors.
[2] Co-equal senior authors.

0142-9612/$ – see front matter © 2013 Elsevier Ltd. All rights reserved.
http://dx.doi.org/10.1016/j.biomaterials.2013.08.033

matrix components lined by endothelia. “Biomatrix scaffolds”, herein referred to as matrix scaffolds, are a particularly rich form of extracellular matrix extracted from organs or tissue and derived from gentle delipidation and perfusion of high salt buffers to keep all collagens and their associated factors insoluble [15]. The organoids can be formed by preparing matrix scaffolds from decellularized livers and then recellularizing the scaffolds with human cells. These matrix scaffolds can be recellularized in two stages: first, the vascular channels are recellularized with endothelia through which medium and then blood can be perfused; and second, the rest of the matrix is recellularized with a combination of hepatic and mesenchymal stem cell populations that will mature into fully functional liver parenchymal cells along with their mesenchymal cell partners. Current efforts are making use of human hepatic cell lines for human liver organoid formation to establish optimal recellularization protocols. Successful protocols will then be used with freshly isolated human hepatic and mesenchymal stem cell populations and endothelia.

For recellularized scaffolds to yield a human liver organoid able to support patients as a bioartificial liver, cell functions must be comparable to those of normal human livers. Since cell seeding and organoid functionality are directly related to the patency and structure of micro-vascular matrix remnants in the scaffold, there is a crucial need for non-destructive assessment of the structural characteristics of the scaffold, particularly its vascular matrix. Without adequate perfusion, the process of reseeding matrix scaffolds with new cells cannot be accomplished, since this process relies on fluid transport through the matrix remnants of the vascular bed for the delivery of the cells. Also, after cells have been engrafted throughout the scaffolds, their continued functions depend on a long-term delivery of nutrients and oxygen. For this reason, a method to image both the anatomy and flow within the sample in a non-destructive manner is highly desirable.

There are many methods currently employed to image tissue scaffolds, including scanning and transmission electron microscopy (SEM and TEM), optical microscopy [6], magnetic resonance (MR) imaging and microscopy [7], computed tomography (CT) [8], optical coherence tomography (OCT) [9], and Doppler ultrasound [10]. The selection of any one modality will always yield inherent tradeoffs such as cost, invasiveness to the sample, field of view, resolution, acquisition time, and type of information gleaned. From this list, the imaging modalities that can non-invasively image a 3D scaffold with a significant thickness are MR, CT, and ultrasound. MR and CT are widely available in both clinical and research contexts. These modalities have the best field of view, although they require expensive hardware (particularly MR imaging). MR can also require long image acquisition times. On the other hand, CT suffers from poor soft-tissue contrast and can cause radiation damage to cells. Ultrasound has many benefits over MR and CT in that it is real-time, relatively inexpensive, non-invasive, does not use ionizing radiation, and has excellent soft-tissue contrast. In addition, ultrasound is able to assess multiple different qualities of a tissue volume (applicable to both *in vivo* volumes and *in vitro* matrix scaffolds), including tissue structure with standard b-mode [11], mechanical stiffness [12], microvascular perfusion architecture [13], and parametric perfusion rate [14]. One possible challenge hindering ultrasound’s utility for scaffold perfusion assessment to date has likely been the modality’s limited field of view, allowing for freehand visualization of different 2D slices, or small 3D sub-volumes, but traditionally not visualization or quantitation of a large field of view. Our objective in this study was to explore the application of ultrasound to perform 3D visualization and quantification of perfusion throughout a matrix scaffold.

In these studies, we have developed a protocol to enable detailed assessment of vascular structural and functional characteristics within scaffolds in a non-destructive manner. We had two objectives: the first was to explore the application of ultrasound to perform 3D visualization and quantification of perfusion throughout an extracellular matrix scaffold; the second was to demonstrate, using a hepatoblast-like cell line, that the imaging assessments can identify scaffolds that will be successful for creating human liver organoids.

2. Materials and methods

2.1. Decellularization of rat livers

Wistar rats (weights 250–300 g) were obtained from Charles River Laboratories, Wilmington, MA, and housed in animal facilities handled by the University of North Carolina (UNC) Division of Laboratory Animal Management. They were fed ad libitum until used for experiments. All experimental work was approved by and performed in accordance with the UNC Institutional Animal Use and Care Committee guidelines.

The protocol for decellularizing livers to produce matrix scaffolds has been described previously [15]. Images of tissue in the process of decellularization are given in the online supplement Fig. S1, and results using this protocol are compared to results using other decellularization protocols (Table S1). Male rats were anesthetized with Ketamine-Xylazine, and their abdominal cavity opened. The portal vein was cannulated with a 20-gauge catheter to provide a perfusion inlet to the vasculature of the liver, and the vena cava was transected to provide an outlet for perfusion. The liver was removed from the abdominal cavity and placed in a perfusion bioreactor. The blood was removed by flushing the liver with 300 ml of serum-free DMEM/F12 (Gibco, Grand Island, NY). A delipidation buffer, comprised of 36 U/L of phospholipase A2 in 1% sodium deoxycholate (Fisher, Pittsburgh, PA) was used to remove plasma and nuclear membranes, and was perfused through the liver for ~30 min (up to an hour) or until the tissue became transparent.

This was followed by perfusion for 90 min with a high salt buffer (NaCL). Solubility constants for known collagen types in liver are such that 3.4 M NaCL is adequate to keep them all in an insoluble state, along with any matrix components and cytokine/growth factors bound to the collagens or the collagen-bound matrix components. The liver was rinsed for 15 min with serum-free DMEM/F12 to eliminate the delipidation buffer and then followed by perfusion with 100 ml of DNase (1 mg per 100 ml; Fisher, Pittsburgh, PA) and RNase (5 mg per 100 ml; Sigma Aldrich, St. Louis, MO) to remove any residual contaminants of nucleic acids from the scaffold. The final step was to rinse the scaffolds with serum-free DMEM/F12 for 1 h to eliminate any residual salt or nucleases. Images are provided in Fig. S1. The decellularized liver scaffolds were stored overnight at 4 °C and perfused with serum-free DME/F12 basal media at 3 ml/min via a peristaltic pump (Masterflex, Cole–Parmer, Vernon Hills, IL) before the imaging study was performed. Prior to an imaging study, the scaffold was transferred from the perfusion bioreactor into the sample imaging chamber (Fig. 1). When in the sample imaging chamber, perfusion was maintained at 4 ml/min through the matrix scaffold remnant of the portal vein via the same peristaltic pump.

2.2. Contrast imaging

An overview of the image data processing workflow is provided (Fig. 2). Flash replenishment imaging was performed using an Acuson Sequoia 512 equipped with a 15L8 transducer (Siemens Medical Solutions USA Inc, Mountain View, CA). The “CPS Capture” software algorithm was used to measure perfusion time. The 3D images of the liver matrix scaffold were acquired by scanning the transducer in the elevational direction using a linear stage and motion controller (UTS150PP and ESP300, Newport, Irvine, CA) interfaced through LabVIEW (National Instruments, Austin, TX) as described by Feingold et al. [14]. Perfusion images were parametrically mapped to contrast arrival times between 1 and 10 s. These images were stored in DICOM format with JPEG compression and analyzed offline in MATLAB (Mathworks, Natick, MA). Perfusion times within the regions of interest were assessed.

Acoustic angiography was performed on a prototype dual frequency probe [16] with imaging parameters previously described [13]. The imaging system was a VisualSonics Vevo770 (Toronto, ON, Canada), with pulses emitted at 4 MHz at 1.23 MPa, and echoes received on a 30 MHz transducer with 100% bandwidth after being passed through a 15 MHz high pass filter to remove non-contrast signal. Three-dimensional images were acquired with the VisualSonics 1D linear motion stage with inter-frame distance of 100 μm to yield nearly isotropic voxels. Images were acquired with a frame rate of 2 Hz, with 5 frames averaged at each location. High resolution b-mode images were also acquired with the Vevo770 system using the same imaging parameters, except the transmit frequency changed to 30 MHz. After imaging, data was exported from the ultrasound system as 8 bit uncompressed AVIs. The microvessels were then segmented from these images using an algorithm originally designed for human magnetic resonance angiography images,

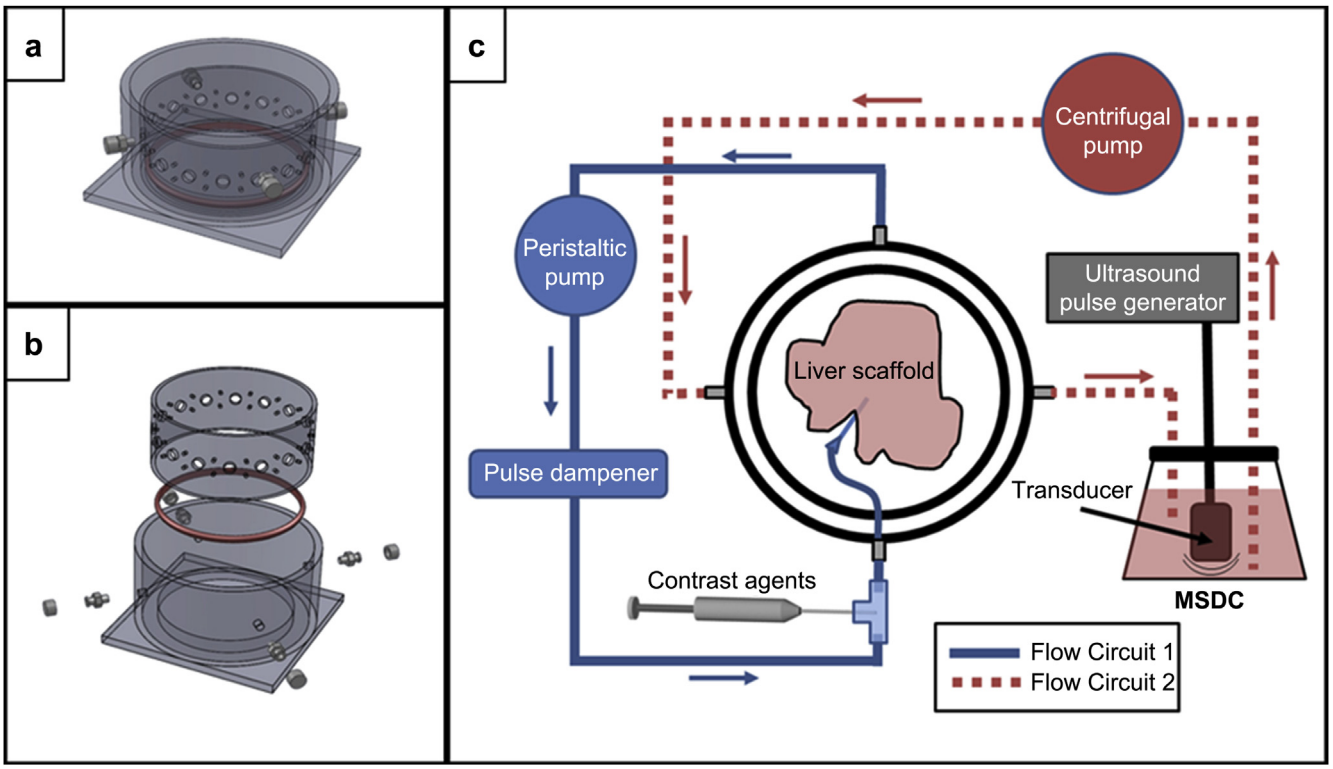

Fig. 1. Schematics for the sample imaging chamber. a) Assembled sample imaging chamber and b) exploded view of the sample imaging chamber. c) A top-down cartoon schematic illustrating the two flow circuits in the setup. Flow Circuit 1 provided perfusion and microbubbles to the liver scaffold, while Flow Circuit 2 provided continuous circulation through the microbubble sequestration and destruction chamber (MSDC) to remove contrast excreted from the sample.

as previously demonstrated by our group [13]. These segmentations yielded XYZ points with subvoxel spacing along vessel centerlines, with estimates of vessel radii at each location. These segmentations were used to assess vessel network architecture.

All three scaffold samples imaged required the registration of multiple sub-volumes for holistic visualization. Perfusion rate information required two sub-volumes for all samples, while the anatomical information and acoustic angiography data required three sub-volumes for sample #1, and two for samples #2 and #3. Once completed, the acoustic angiography data was displayed via maximum intensity projections (MIPs) (Fig. 3). Anatomical b-mode data cannot be displayed in this fashion, so XZ slices through the merged volumes were displayed.

2.3. Imaging the matrix scaffolds

Image acquisition for each sample (Fig. 4, Panels 1 and 2) required approximately 50 min total, due to the small step sizes used in each case to obtain high resolution images (800 μm steps for the anatomical and perfusion images, and 100 μm steps for the acoustic angiography). Standard grayscale ultrasound images provided reference for the scaffold "anatomy" but provided no functional information. Acoustic angiography provided high-resolution images of the branching microvasculature structure, with no tissue background. Perfusion imaging provided spatial distributions of local flow rates (images not shown). All image sets were co-registered using major anatomical landmarks. Total field of view for the regions of interest acquired was approximately 4 × 4 × 3 cm (axial × lateral × elevation) for the anatomical and perfusion images, and approximately 4 × 3 × 1.4 cm for the acoustic angiography.

2.4. Scanning electron microscopy (SEM)

Samples of normal rat liver versus rat liver matrix scaffolds were fixed with 4% buffered formaldehyde and examined by SEM at high vacuum (Quanta 200 Field Emission Gun, FEI™, Hillsborough, OR) at the Chapel Hill Analytical and Nanofabrication Laboratory on the UNC campus.

2.5. Recellularization of matrix scaffolds

Matrix scaffolds with intact vasculature were seeded with human hepatoblast-like cells, Hep3B cells (ATCC® HB-8064™). These cells were introduced by perfusion through the matrix remnants of the portal vein via a peristaltic pump (see Fig. S3) and cultured in Hep3B medium (DMEM + 10% Fetal Bovine Serum). Approximately 130×10^6 cells were perfused into a scaffold in steps with 20 min intervals. During each interval, 30×10^6 cells were perfused at 15 ml/min for 10 min, followed by 10 min of rest (0 ml/min). This was repeated 4 times. Once all of the cells were introduced into a matrix scaffold, the flow rate was lowered to 1.3 ml/min and the scaffolds were perfused with the culture medium. The medium was changed after 24 h and again every 3 days.

The reseeded matrix scaffolds were cultured in the bioreactors (Fig. S3) for up to 14 days. After 14 days, lobes of the reseeded matrix scaffold were either frozen for histology and immunohistochemistry, or fixed for scanning electron microscopy (SEM) imaging (using the method noted above). Sections of the reseeded matrix scaffolds were assessed also by immunohistochemistry and immunofluorescence for cell distribution (Hematoxylin and Eosin), cell proliferation (Ki67) and apoptosis, as well as for albumin and urea protein expression. SEM images were also taken to view cell location with respect to vasculature. Antibody information and dilutions are provided in the Supplemental materials.

3. Results

3.1. Sample imaging chamber

In order to image the delicate tissue scaffold, a chamber (Fig. 1) was designed to allow a tissue sample to be imaged while submerged in media, since ultrasound imaging at the frequencies utilized requires coupling of the imaging transducer to the sample with liquid. The fluid bath allows for non-contact image acquisition, as opposed to gel-based coupling that is typical for ultrasound imaging exams, while preserving the hydration of the scaffold. Because there was no contact pressure between the tissue and the imaging transducer, tissue was not deformed during imaging; this resulted in better registrations of multiple sub-volumes of image data.

The imaging chamber designed for this purpose was composed of two concentric 0.25 inch thick acrylic cylinders, each 3 inches tall. The outer diameters of the outer and inner

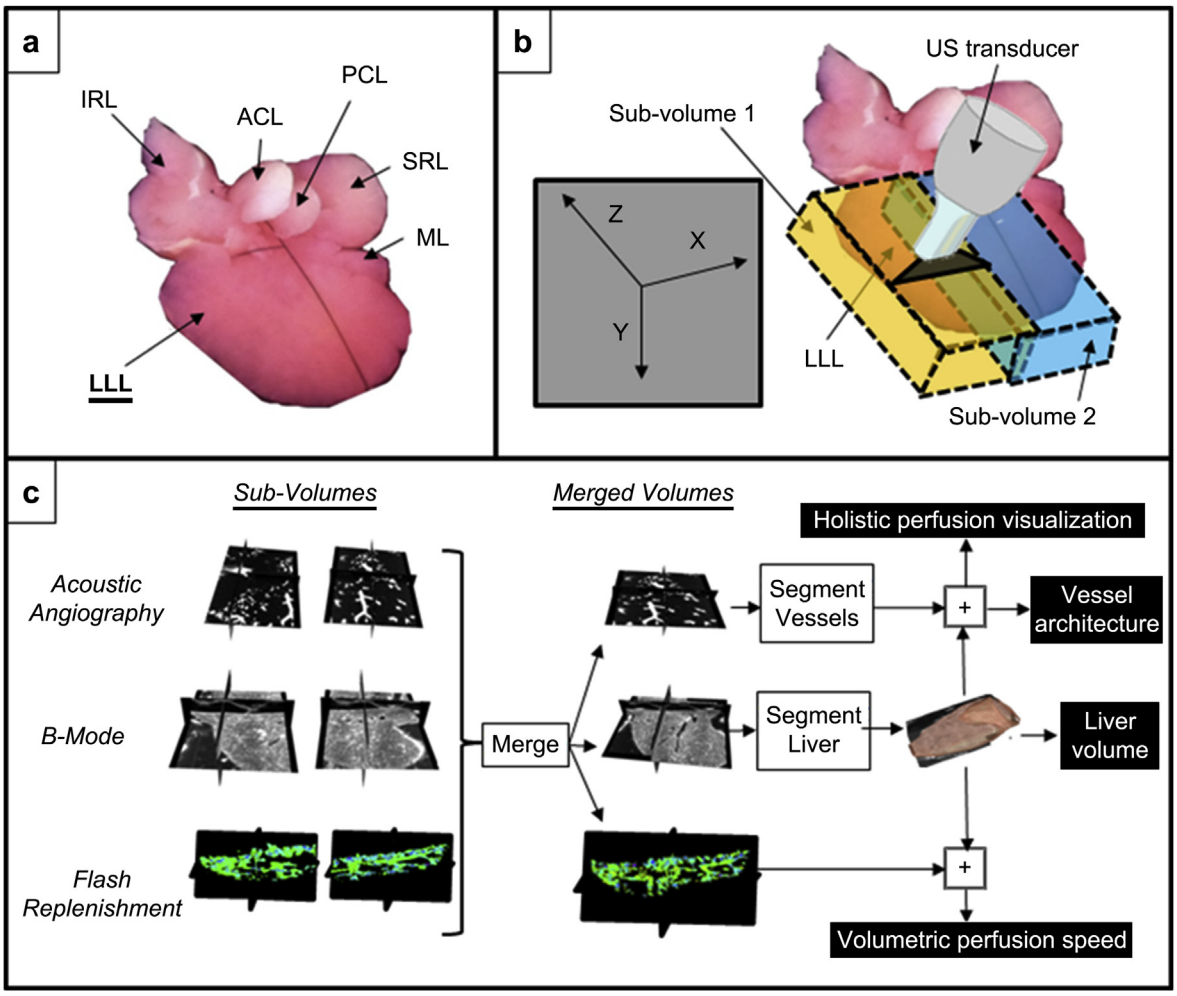

Fig. 2. The orientation of the matrix scaffold sample as viewed from above with the following visible lobes labeled: a) left lateral lobe (LLL), inferior right lobe (IRL), anterior caudate lobe (ACL), posterior caudate lobe (PCL), superior right lobe (SRL), and median lobe (ML). The LLL was the lobe imaged in this study. Lobes were identified in this figure via an available surgical guide. b) Orientation of the imaging sub-volumes relative to the tissue sample. XY dimensions were lateral and axial axes within the ultrasound coordinate space, with the *Z*-axis being the elevational scan direction. c) Schematic explaining the registration of multiple 3D volumes from three distinct ultrasound imaging approaches into the final composite volume.

cylinders were 6 and 5 inches, respectively. The outer cylinder was mounted to the 6 × 6 × 0.3 inch acrylic base of the imaging chamber using acrylic glue. The inner cylinder was fit to the imaging chamber's base over a Vaseline-lubricated silicone O-ring to allow for quick coupling with a tight seal. Though not implemented in this study, this O-ring design also enables bi-directional imaging orientations (*i.e.* it is possible to rotate the inner chamber and image the contralateral side of the tissue sample). The interior cylinder served several purposes. It provided a frame for the tissue sample support webbing, made from 5.0 silk sutures (Ethicon, Somerville, NJ). This support webbing held the sample suspended in the interior of chamber. Additional suture was loosely tethered over the top of the tissue to prevent flotation or shifting during the imaging study. The interior cylinder of the sample imaging chamber also allowed for efficient buffer circulation but limited turbulence near the sample.

Preliminary studies showed that the peristaltic pump, which powered flow circuit #1, caused a slight periodicity in the flow rate through the scaffold samples as a result of the pump's rotary wheel design; this affected perfusion measurements. To prevent this artifact, a pulse dampener (Model 07596-20, Cole–Parmer, Vernon Hills, IL) was placed between the output from the peristaltic pump and the input to the sample. Preliminary studies also showed that contrast agent exiting the sample into the surrounding fluid after perfusing through the portal circuit resulted in a decrease in image quality over time as contrast agent floated between the imaging transducer and the sample. To prevent this, a clearance fluid circuit was implemented (Fig. 1). This circulated the fluid surrounding the scaffold sample though a microbubble sequestration and destruction chamber (MSDC) before reinjection into the imaging chamber. The MSDC was a 2 L Erlenmeyer flask in which a 1 MHz unfocused piston transducer was suspended (Valpey-Fisher, Hopkinton, MA) to facilitate contrast destruction. The 1 MHz piston transducer was pulsed at 10 Hz with a pressure of 460 kPa via a pulser (Model 801A, Ritec, Warwick RI). Under these conditions, free contrast agent in the solution flowing through the chamber was destroyed and thus removed from the circulating media. Media surrounding the scaffold was continually pumped through this chamber at 1 ml/min using a centrifugal pump (Model PQ-12, Greylor, Cape Coral, FL) powered by an external DC power supply (Model DIGI360, Electro Industries, Westbury, NY). Four nylon luer fittings were attached to the outer cylinder for coupling the sample imaging chamber to the two flow circuits. All fluid circuits used 0.125 inch inner diameter Tygon tubing, except between the catheter entering the scaffold sample and the outer cylinder of the imaging chamber (0.062 inch in diameter).

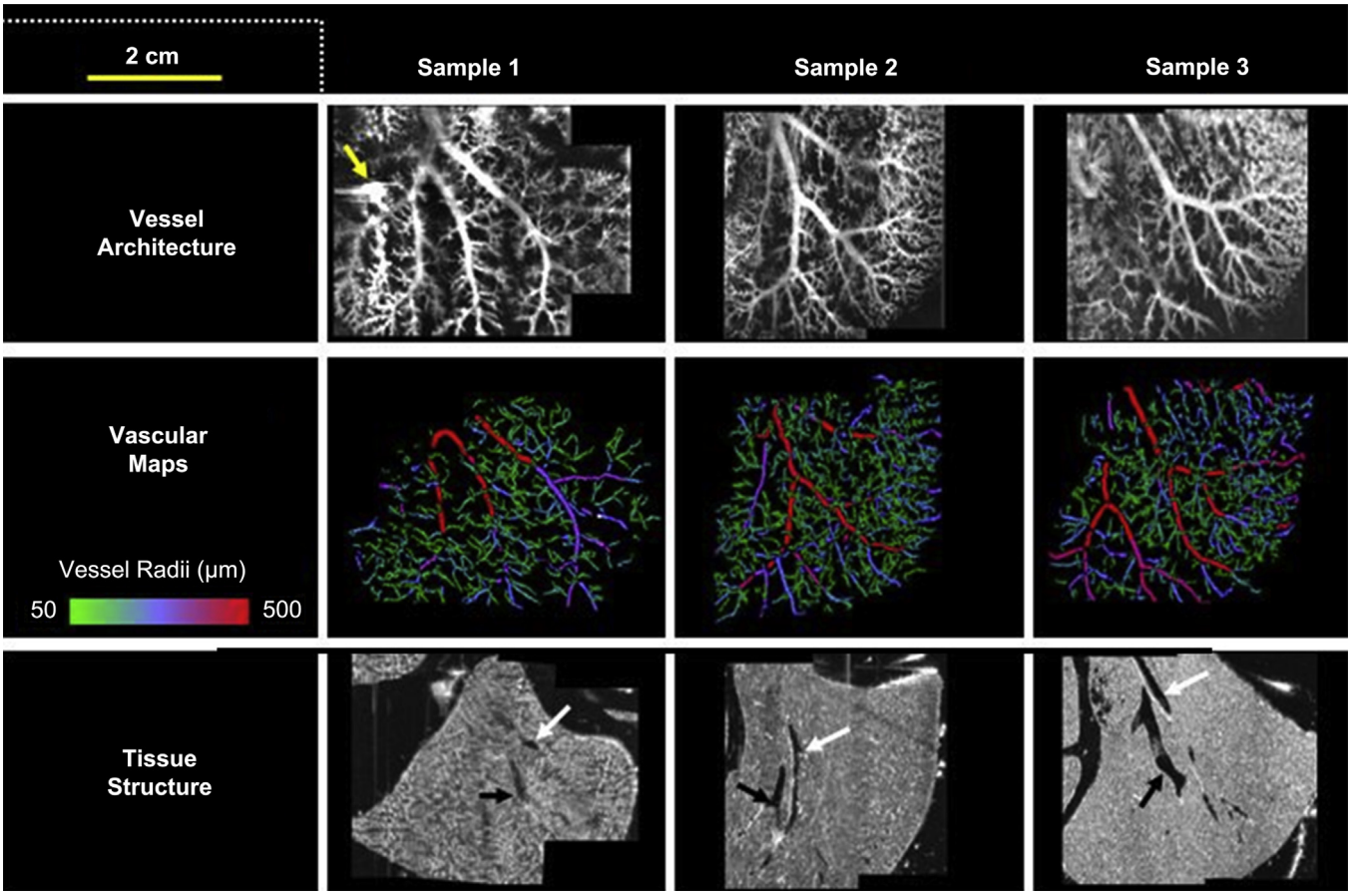

Fig. 3. A compilation of image data acquired of the three matrix scaffold samples. Yellow arrow indicates location of sample #1, which was perforated and thus leaking microbubbles. Each row was acquired with the following imaging modes (from top to bottom): Acoustic angiography, semi-automated segmentations from acoustic angiography data, and b-mode. White and black arrows on the b-mode images indicate vessels identified as part of either the portal or hepatic circuits, respectively. (For interpretation of the references to color in this figure legend, the reader is referred to the web version of this article.)

The microbubbles used in this study were prepared as previously described [17]. Microbubbles were introduced to the perfusion fluid circuit through a T-valve injection port located between the pulse dampener and the matrix scaffold. A 24-gauge needle was used to pierce the septum, and microbubbles could then be injected into the fluid circuit via a computer-controlled syringe pump (Harvard Apparatus, Holliston, MA). Microbubbles were administered into the fluid circuit at a concentration of 1.5×10^9 per mL in a 1 cc syringe and at a rate of 20 μL/min.

Three liver matrix scaffolds were imaged (Fig. 3), hereafter referred to as samples 1 through 3. The left lateral lobe (LLL) of each scaffold was selected as the lobe of interest, because it is easily accessed for imaging. Another advantage is its narrow morphology; the Vevo770 has a fixed acoustic focus, and thus has a narrow depth of field (<1 cm). Our goal was to provide a holistic assessment of perfusion throughout a volume of tissue, and the left lateral lobe was most amenable to this objective. It should be noted that the techniques presented here could be extended to the entire volume of tissue using a transducer with a larger axial field of view. Each liver matrix scaffold was imaged with two contrast imaging modes: flash replenishment and acoustic angiography.

3.2. Registration of sub-volumes

Because the lateral field of view of the ultrasound transducers used for these imaging studies was insufficient to capture the entirety of the liver lobe of interest, multiple sub-volumes were acquired on each system and later registered together offline. The term "sub-volume" is used to describe a 3D volumetric image that does not holistically capture a tissue of interest. Registration of these sub-volumes was performed within the open source 3D Slicer environment (ver 4.2.1, National Alliance for Medical Image Computing) using the MergeAdjacentImages module, part of the TubeTK extension. This module is designed to register together two images that have a small degree of overlap along one of the axes. When the sub-volumes were registered together using the Merge module, they formed a single cohesive volume for the liver lobe of interest for each image type (b-mode, flash replenishment, and acoustic angiography). The transform module was then used to register the three types of ultrasound image data to each other, creating a single composite 3D image for each of the livers imaged.

3.3. Grayscale anatomical imaging

Grayscale imaging (*i.e.* the standard non-contrast enhanced imaging) enabled tissue visualization for 3-dimensional region of interest (ROI) segmentations. These data were utilized to calculate tissue volumes of the left lateral lobe (LLL), which were 7.24, 5.93, and 7.79 mL for samples #1–3, respectively.

3.4. Acoustic angiography

Vessel network architecture was assessed using more than 1700 vessel segmentations extracted from the acoustic angiography

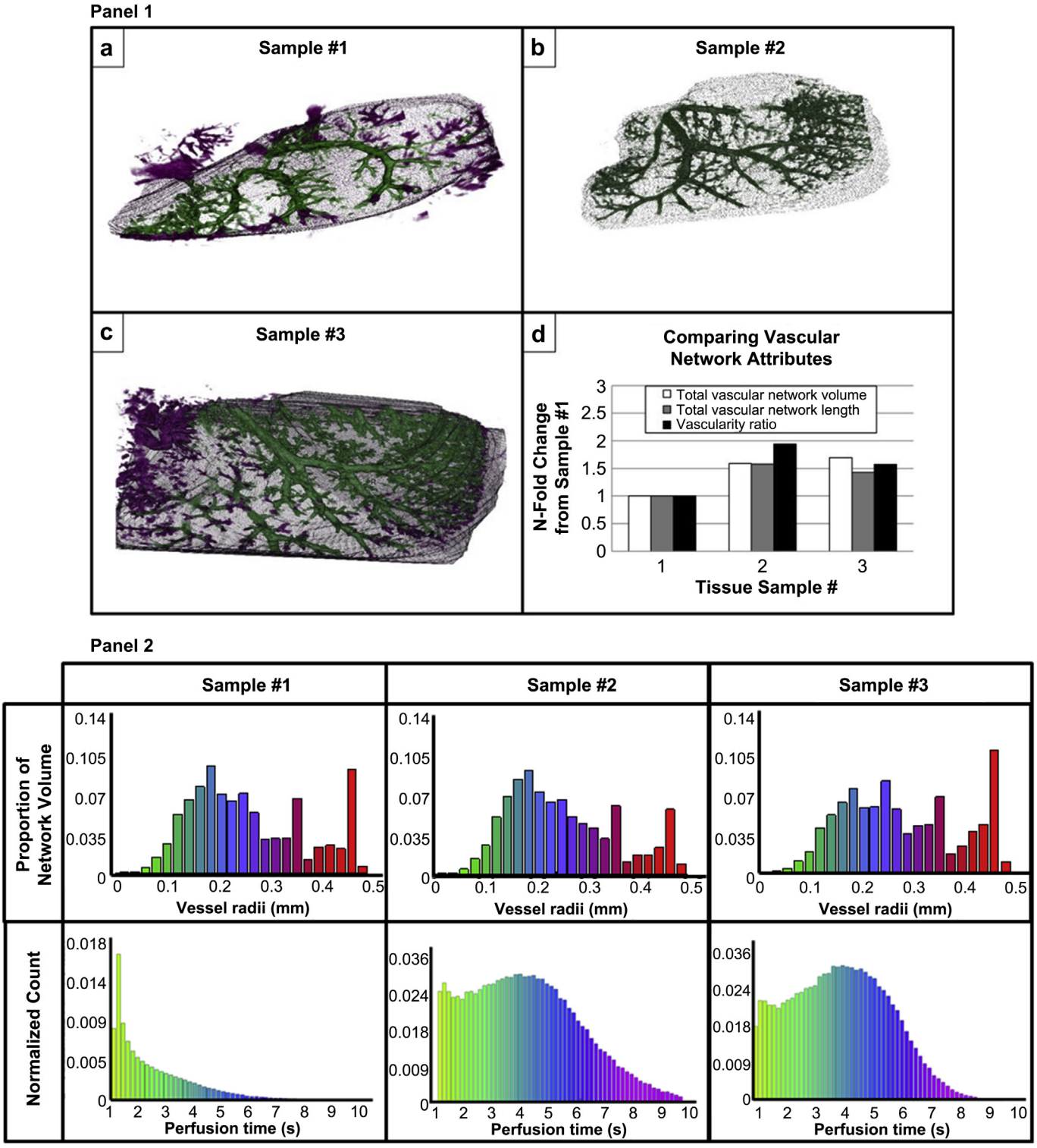

Fig. 4. Panel 1. a–c) 3D renderings of the matrix acoustic angiography data. Color is defined as either inside (green) or outside (purple) of the manually defined tissue border. d) Quantitative assessments of vascular network volume, length, and vascularity ratio. Data are normalized to sample #1. Panel 2. Perfusion comparisons between the three liver scaffolds evaluated from the flash-replenishment imaging. (Top) Area normalized vessel size histograms computed from the vessel segmentations. (Bottom) Area normalized perfusion rate histograms. (For interpretation of the references to color in this figure legend, the reader is referred to the web version of this article.)

image data. These data were rendered in 3D and color coded based on whether vessels are inside or outside the manually defined tissue boundary (Fig. 4, Panels 1 and 2). Different numbers of vessels were extracted from each sample: for sample #1 ($N = 415$ vessel segmentations), sample #2 ($N = 702$ vessel segmentations), and sample #3 ($N = 671$ vessel segmentations). The volumes of these vessel network segmentations were computed to be 142.6, 226.6, and 241.3 μl, and the total lengths were computed to be 1.0245, 1.6177, and 1.4646 m for samples #1, #2, and #3, respectively.

The vascularity ratios were 1.97%, 3.82%, and 3.10% for samples #1, #2, and #3, respectively (Fig. 4, Panel 1d). Although these metrics revealed sample #1 to contain fewer perfused vessels (both in total volume of the vessel network, and as a proportion of total volume of the matrix scaffold) the distribution of vessel sizes were similar between all three samples (Fig. 4, Panel 2 – top).

3.5. Perfusion imaging

The perfusion values within each volume were assessed using regions of interest as defined based on anatomical data. Histograms of the perfused pixels within the scaffold volumes were computed and plotted as a function of perfusion time (Fig. 4, Panel 2 – bottom). Samples #2 and #3 had similarly shaped histograms with similar mean perfusion times of 3.128 ± 1.923 s, and 3.017 ± 1.677 s (mean $\mu \pm \sigma$), respectively. Sample #1, on the other hand, had a negatively skewed monotonically decreasing histogram with a mean perfusion of 1.381 ± 1.328 s. This result was in alignment with the differences in the perfusion images, which could be qualitatively observed; sample #1 had a larger proportion of faster perfusing regions than samples #2 and #3 (Fig. 4).

3.6. Scanning electron microscopy of intact liver vs. matrix scaffolds

Scanning electron microscopy (SEM) of liver versus matrix scaffolds (Fig. 5, Panel 1, 5a and 5b) indicated that the decellularization protocol preserves the liver's histological infrastructure, and that the macro- and micro-vascular channels are clearly intact in the liver matrix scaffolds (see arrows). These SEM images are complemented by our prior studies showing that all known extracellular matrix components, including all known collagen types, are present and preserved at >98% of the levels found in normal liver, and that the scaffolds are negligible for nucleic acids and for cytoplasmic components [15]. All known matrix components in liver versus scaffolds were assessed by immunohistochemistry and found to be in their correct histological sites, meaning that the liver acinar zonation (zones 1–3) is preserved in terms of gradients of matrix components [15,18].

3.7. Engraftment efficiency of scaffold recellularization

As a proof-of-concept towards human liver organoid formation, matrix scaffolds with patent vasculature were reseeded with approximately 130×10^6 Hep3b cells, human hepatoblast-like cells of a hepatic cell line (ATCC® HB-8064™). This cell line was established by Barbara Knowles and associates from a tumor from an 8-year old patient [19] and has been extensively characterized with respect to liver-specific gene expression by Darlington and associates [20]. The Hep3B cells were introduced into the matrix scaffold by perfusion through the matrix remnants of the portal vein using a peristaltic pump. The cells attached within minutes, and engraftment efficiency was near 100% by the end of the seeding process.

Over the course of 14 days, the medium from bioreactors with reseeded scaffolds was collected at varying time points and assayed by ELISA for secreted products (Fig. 6). At the end of the 14 day culture period, scaffolds were evaluated by SEM, histology and immunohistochemistry. SEM images (Fig. 5, Panel 1) show cells that have engrafted onto or into the matrix scaffold. Hematoxylin and eosin stained sections revealed a wide cell distribution throughout the scaffolds (Fig. 5, Panel 2, 5a). The seeded cells actively proliferated throughout the 14 days of culture, as demonstrated by Ki67 staining (Fig. 5, Panel 2, 5b), but they did not show any evidence of apoptosis (data not shown). In addition, the reseeded cells expressed liver-specific proteins in patterns correlated with their known locations in the normal liver acinus *in vivo*. Albumin (Fig. 5, Panel 2, 5c) was found in all of the cells but at higher levels in regions of the scaffolds correlated with acinar zones 2 and 3, whereas epithelial cell adhesion molecule, EpCAM (Fig. 5, Panel 2, 5d), was expressed only by cells clustered near the matrix remnants of portal triads, acinar zone 1. EpCAM is a marker of hepatic stem/progenitors {15}. Hep3B cells have phenotypic traits indicating that they are hepatoblast-like [20]; normal hepatoblasts are found only in zone 1 of the pediatric and adult liver acinus, and are at a lineage stage in which EpCAM is a key phenotypic trait.

4. Discussion

We describe a method of imaging for the evaluation of matrix extracts prepared by decellularization of tissues. Our techniques may provide important information regarding vascular patency, which is particularly important if such scaffolds are to be used as substrata for cell populations as part of organoid formation. The ultrasound images described here provide insights into the complexity of the matrix remnants of the liver architecture and of the vascular channels. The dimensions of the channels can be quantified precisely using these ultrasound technologies and corresponding segmentation algorithms, enabling the identification of categories of blood vessels for which such dimensions are known (up to 100 μm). Furthermore, these techniques provide a non-destructive method to assess vascular functionality.

When using ultrasound, contrast agents are utilized to image and quantify flow in microvessels, due to the poor acoustic contrast from blood. Microbubble contrast agents are the predominantly used vascular contrast agent for ultrasound. They are micron-sized lipid encapsulated gaseous spheres which, when immersed in a fluid, provide a strongly reflective interface and thus a high degree of contrast in an ultrasound image. Microbubble contrast agents (diameters typically between 1 and 5 μm) are much larger than vascular fenestrations, which allow them to remain within the luminal space. At the same time, they are small enough to pass through capillary beds. Since their rheology is similar to red blood cells [21], they are a suitable contrast agent for spatial mapping of vascular channel networks within matrix scaffold networks, thereby serving as surrogate markers for mapping cell movement within the scaffold.

In addition to traditional "grayscale" ultrasound to provide reference images of the scaffold physical structure, two different contrast-enhanced ultrasound techniques were utilized in this work to provide functional information about matrix scaffold microvasculature. The first technique, referred to as "flash replenishment", or "dynamic contrast-enhanced perfusion imaging" (DCE-PI), allows relative blood perfusion to be spatially mapped by assessing the speed at which contrast agents refill a sample volume after clearance [22]. While this technique is not new, it has not previously been performed in this type of scaffold imaging application.

The other contrast imaging approach implemented in this study is a technique we refer to as "acoustic angiography". This newly developed imaging method differs from traditional ultrasound imaging in that it is designed to visualize vascular and micro-vascular structure at high resolution rather than tissue anatomy [16,23]. Unlike flash replenishment, acoustic angiography does not yet have the ability to parametrically map perfusion rates. However, it can provide detailed visualization of vessel architecture and provide a high resolution dataset from which vessels can be segmented and quantitatively mapped (vessel network volume, length, etc.). High resolution acoustic angiography requires a new type of transducer developed by our lab with collaborators in F. Stuart Foster's group at the University of Toronto, Sunnybrook [16] that is not yet available on

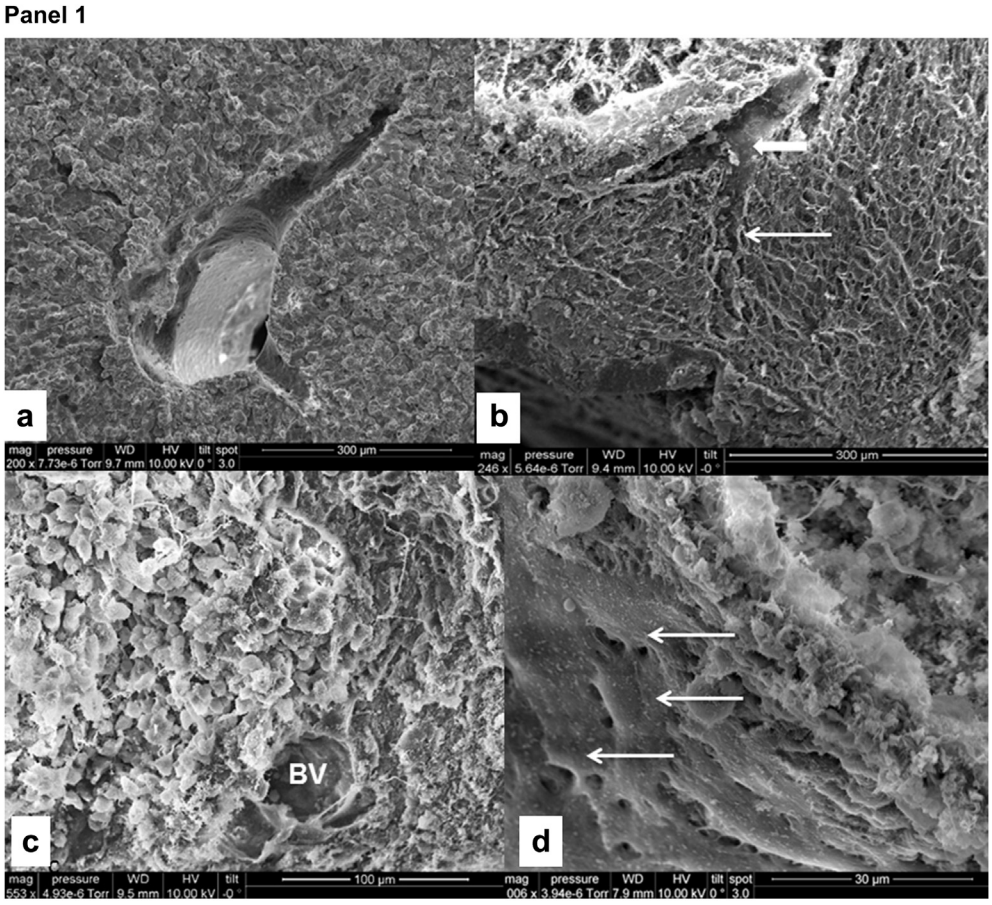

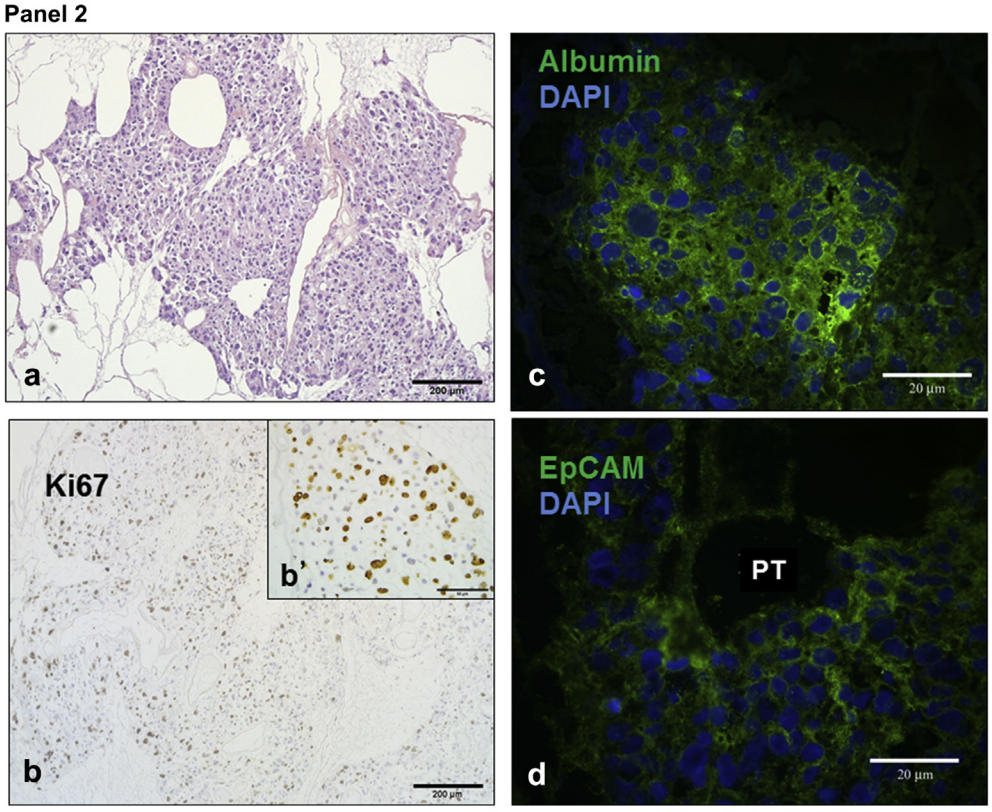

Fig. 5. Panel 1. Scanning electron microscopy (SEM) of a) normal adult rat liver fixed with 4% paraformaldehyde and subjected to SEM; b) normal rat liver matrix scaffold. The major and minor vascular channels are evident in both the liver and in the scaffold. Empty spaces are visible where parenchymal cells previously resided (thin arrow). Major vascular

commercial ultrasound systems. The protocol utilized for this work involves three imaging scans: the first defines the scaffold's physical structure (anatomy) with standard "b-mode" or grayscale ultrasound as is commonly used clinically; the second maps vessel architecture with high resolution acoustic angiography for vascular network visualization and quantitation; the third maps perfusion rates with flash replenishment. All three studies could be performed sequentially with appropriate system hardware.

The analyses of these scaffolds by imaging modalities provide evidence for the complexity of the matrix remnants of the liver architecture and of the vascular channels, as well as evidence of the scaffolds' biological efficacy. These analyses also provide assistance with recellularization protocols. The dimensions of the channels can be quantified precisely using these ultrasound technologies and corresponding segmentation algorithms; this enables identification of categories of blood vessels for which such dimensions are known.

From a quantitative standpoint, sample #1 was noticeably different from samples #2 and #3 in both the acoustic angiography and perfusion images. Sample #1 illustrated a similar vessel size distribution to the other two samples, but showed a grossly reduced perfusion rate. This was due to a defect in sample #1 – the scaffold was damaged, resulting in several low resistance outlets for flow exiting the system. Although we were not able to perceive this damage prior to imaging, it was clearly reflected in the functional data. One perforated outlet was clearly visible within the acoustic angiography image set (Figs. 3 and 4, Sample 1, yellow arrow).

Furthermore, during contrast infusion, it was possible to delineate vessels as part of either the hepatic or portal circulatory networks within the tissue volume (Fig. 3, white vs. black arrows, respectively). Because contrast was infused though the portal vein, the hepatic circuit did not contain contrast and thus was not visualized under acoustic angiography. When the b-mode volumes were registered to the acoustic angiography volumes, flow voids in the b-mode, which were not perfused within the acoustic angiography dataset, could be classified as components of the hepatic circuit. Alternatively, we could have perfused the hepatic and portal circuits separately, although this was not done in our experiments for simplicity.

The ultrasound approaches we describe offer a non-destructive, high resolution, and potentially inexpensive technique for visualization of scaffold perfusion. Additionally, these approaches offer a better depth of penetration into the scaffold than optical imaging approaches, allowing for the visualization of the entirety of the LLL (at the expense of both axial and lateral resolution, which is worse than systems imaging at optical wavelengths).

While the advantages of this protocol are numerous, there are also several drawbacks to this approach. Currently, the imaging technology presented for the acoustic angiography vessel mapping is not commercially available. Also, while several groups have made strides toward calibrating flash replenishment imaging against gold standards for perfusion rate [22,24], the technique currently provides only relative quantitative measures for perfusion. This is adequate for assessing differences in regions within a given sample, such as would be necessary for identifying pockets of occlusion. It does not yet allow determination of absolute flow rates ($mL\,s^{-1}\,cm^{-3}$) within the scaffold without prior calibration based on the tissue volume. Finally, our technique was relatively slow, due to the 1-D form factor of our transducers, which were able to image only a single 2-D image slice at a time and required us to mechanically scan the transducers across the tissue volume. The 2-D matrix ultrasound transducers now in development are able to acquire entire image volumes at a much higher frame rate, although transducers required to perform real-time 3D contrast imaging at the resolution described here are not yet commercially available.

The rapid and successful recellularization of the scaffolds with the Hep3b cells demonstrated the patency and functionality of the matrix remnants of the vascular network. It is interesting that, although the vascular walls remain sufficiently patent to constrain 1-5 micron microbubble contrast agents, the cells were still able to cross the matrix remnants of the vascular channels and engraft into all parts of the matrix, including that associated with parenchymal cells (Fig. 5, Panel 1, 5c). It is unclear how the cells were able to engraft after seeding by perfusion into a decellularized liver, since the matrix remnants of the vascular channels were intact. Many researchers who have successfully seeded cells into decellularized organs used decellularization protocols that destroyed facets of the vascular matrix [25]. Of those using protocols resulting in patent vascular channels ([26], it has never been explained how the cells are able to breach patent vascular matrix walls and engraft. Baptista et al. [26] hypothesized that their method of decellularization by harsh detergents followed by distilled water perfusion may have caused structural damage to the vascular architecture such as thinning of the matrix or creating small holes; this might, in turn, have allowed cells to migrate across the permeabilized walls.

We have confirmed that our decellularization method results in intact scaffolds without evidence of a defect: there were no breaches of the vascular matrix greater than 5 microns prior to seeding. An alternative explanation for the cells' ability to breach matrix walls and engraft derives from hepatocyte transplantation studies [27,28]. In these studies it was shown that sinusoidal endothelial cells can shift to allow the hepatocytes access to larger fenestrae through which they achieve access and integrate into the parenchymal cell plates. SEM imaging of our reseeded scaffolds suggest that cells are attaching to and engaging the matrix and perhaps are able to squeeze through residual fenestrae left behind after decellularization (Fig. 5, Panel 1, 5d, arrows).

Non-destructive 3D perfusion imaging of decellularized organs and tissues could have significant value in tissue engineering investigations and also in tracking recellularization. Contrast ultrasound techniques have been shown to have utility in measuring microvasculature structural information and relative flow rate correlated with anatomical orientation in tissue scaffolds. The recellularization studies presented here indicate that cells are successfully being delivered and engrafting into the matrix remnants of the liver parenchyma by perfusion seeding (Fig. 5, Panel 2). This perfusion seeding method is only possible in a patent vascular

channels are also visible (thick arrow); c) low magnification image of rat liver matrix scaffold reseeded with Hep3b cells. Large numbers of cells are found bound to the matrix throughout the scaffolds. This attachment occurs within minutes of seeding the cells and results in near 100% engraftment by the end of the seeding process; d) Higher magnification image of rat liver matrix scaffold showing Hep3b cells that have attached, spread and are forming classic cellular extensions and connections with each other. They engage (thick white arrow) the lumen of the vessel wall and perhaps pass through the fenestrae (thin white arrow) that remain following decellularization. Panel 2. a) Hematoxylin and eosin stained sections revealed a cell distribution throughout the matrix scaffolds. b) The seeded cells actively proliferated through day 14, demonstrated by Ki67 staining (seen in magnified version in b'). c) The Hep3b cells expressed peak albumin levels (albumin = green, DAPI = blue) in regions of the matrix scaffolds correlated with zones 2 and 3 of the liver acinus. d) Cells bound to matrix remnants of the portal triads (zone 1) expressed albumin more weakly than elsewhere on the matrix. By contrast, EpCAM expression was quite strong in the cells bound in these regions but weak or negligible if in matrix regions associated with zones 2 and 3 (EpCAM = green, DAPI = blue). This is surprising, given that the test cells are a cell line and yet they apparently still have the capacity to show some degree of zonation of functions if bound to specific regions of the matrix scaffolds. (For interpretation of the references to color in this figure legend, the reader is referred to the web version of this article.)

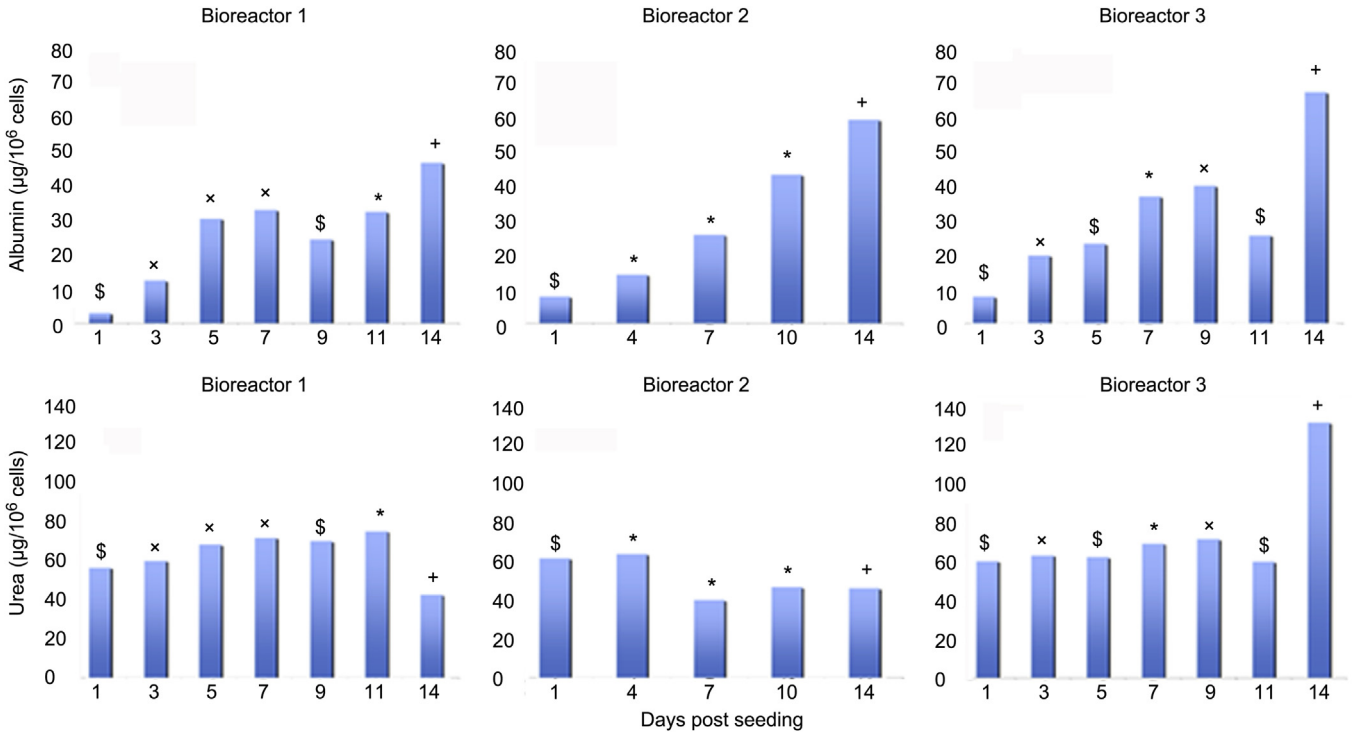

Fig. 6. Measurements of albumin and urea secretion by Hep3B cells seeded in matrix scaffolds ($n = 3$) and cultured over a 14-day period. Levels are normalized to the number of initial number of cells seeded into the scaffold. Symbols indicate media collection over 24 h ($), 48 h (×), 72 h (*), and 96 h (+). Statistical analyses were unable to be performed, and, therefore, raw data are presented.

network, which is confirmed through the use of this high resolution acoustic angiography technology. Ongoing current studies include the correlation of structural information, such as vessel diameters, perfusion rates, local fluid shear rates, and patency with the gold standard of histological data after recellularization procedures are complete. Also, ligand-bearing microbubbles could be implemented to perform 3D ultrasonic molecular imaging, which can be used to spatially map specific regions of cell attachment and cell differentiation using biomarkers [13] and thus could be used to detect spatial distributions of different types of cells or varying biological states of cells in the scaffold.

Extracellular matrix scaffolds prepared by decellularization protocols are central to the strategies for organoid formation, since individual and purified matrix components give only partial effects in induction and maintenance of differentiated cells. Efforts to isolate successful matrix scaffolds have dominated recent investigations [25,26,29–33]. All of the protocols have proven successful in isolating matrix extracts dominated by cross-linked collagens. However, most do not generate scaffolds with patent vasculature [25,29], or they yield scaffolds in which uncross-linked, nascent collagens and associated matrix components are lost [26]. The protocol we present here preserves both the cross-linked and the uncross-linked nascent collagens and preserves more of the adhesion molecules, proteoglycans and growth factors/cytokines that are bound to these matrix components [15]. The proof-of-principle studies with Hep3B cells indicate that the richer matrix extracts such as the matrix scaffolds confer very rapid attachment (within minutes), near 100% engraftment, and significant induction of tissue-specific functions (to the extent possible with a transformed hepatic cell line).

Human liver organoids are being established for use as bioartificial livers through which a patient's blood can be perfused for detoxification and synthesis of critical liver-specific products. We have previously shown that normal liver cells bound to frozen sections of matrix scaffolds and maintained in a serum-free, hormonally defined media designed for mature cells are fully functional and stable *ex vivo* for months [15]. If this proves true for the scaffolds used intact (*i.e.* not as frozen sections) for organoid formation, when these scaffolds are recellularized with freshly isolated human cells they will offer opportunities for liver-assist devices for patients. They also will offer the potential to generate grafts for transplantation into patients.

5. Conclusions

Non-destructive 3D perfusion imaging of decellularized organs and tissues has significant value in tissue engineering investigations and also in tracking recellularization processes of matrix scaffolds in organoid formation. Contrast ultrasound techniques have been shown to have utility in measuring microvasculature structural information and relative flow rate correlated with anatomical orientation in tissue scaffolds. The recellularization studies presented here indicate that cells are successfully being delivered and engrafting into intact scaffolds by perfusion seeding. This perfusion seeding method is only possible in a patent vascular network, a finding that is confirmed through the use of this high resolution acoustic angiography technology.

Acknowledgments

We thank Dr. V Madden and Wallace Ambrose for TEM and SEM processing, Dr. Jim Tsuruta for contrast agent formulation, Carlton W. Anderson for ELISA analysis (grant NIDDK P30 DK34987), Eliane Wauthier for lab management, and Lucendia English for lab support. The authors declare no conflict of interest. Relevant support for the Dayton Lab has been provided by the National Institutes of Health through grants R01CA170665 and 1R43CA165621. RCG is supported by an NSF Graduate Research Fellowship. Support for the Reid Lab is

derived from an SRA from Vesta Therapeutics (Bethesda, MD), an SRA from the Hamner Institute (a subcontract of a grant from the Dow Chemical Company), and from an NCI grant (CA016086). Patent applications on matrix scaffolds have been filed, are owned by UNC and have been licensed to *PhoenixSongs Biologicals* (Branford, CT) for non-clinical uses and to Vesta Therapeutics (Bethesda, MD) for clinical programs. Kitware, Inc. has been provided funding through the National Institutes of Health 1R43CA165621.

Appendix A. Supplementary data

Supplementary data related to this article can be found at http://dx.doi.org/10.1016/j.biomaterials.2013.08.033.

References

[1] Puppi J, Strom SJ, Hughes RD, Bansal S, Castell JV, Dagher I, et al. Improving the techniques for human hepatocyte transplantation: report from a consensus meeting in London. Cell Transplant 2012;21:1–10.
[2] Smith JM, Biggins SW, Haselby DG, Kim WR, Wedd J, Lamb K, et al. Kidney, pancreas and liver allocation and distribution in the United States. Am J Transplant 2012;12:3191–212.
[3] Gerlach JC, Zeilinger K, Patzer JF. Bioartificial liver systems: why, what, whither? (Review). Regen Med 2008;3:575–95.
[4] Catapano G, Patzer JF, Gerlach JC. Transport advances in disposable bioreactors for liver tissue engineering. Adv Biochem Eng Biotechnol 2010;115:117–43.
[5] Macdonald J, Griffin J, Kubota H, Griffith L, Fair J, Reid LM. Bioartificial livers. In: Kuhtreiber WM, Lanza RP, Chick WL, editors. Cell encapsulation technology and therapeutics. Boston: Birkhauser; 1999. p. 252–86.
[6] Smith LE, Smallwood R, MacNeil S. A comparison of imaging methodologies for 3D tissue engineering. Microsc Res Tech 2010;73:1123–33.
[7] Xu H, Othman SF, Magin RL. Monitoring tissue engineering using magnetic resonance imaging. J Biosci Bioeng 2008;106:515–27.
[8] Young S, Kretlow JD, Nguyen C, Bashoura AG, Baggett LS, Jansen JA, et al. Microcomputed tomography characterization of neovascularization in bone tissue engineering applications. Tissue Eng Part B Rev 2008;14:295–306.
[9] Liang X, Graf BW, Boppart SA. Imaging engineered tissues using structural and functional optical coherence tomography. J Biophotonics 2009;2:643–55.
[10] McGuigan AP, Sefton MV. Vascularized organoid engineered by modular assembly enables blood perfusion. Proc Natl Acad Sci U S A 2006;103:11461–6.
[11] Foster FS, Zhang MY, Zhou YQ, Liu G, Mehi J, Cherin E, et al. A new ultrasound instrument for in vivo microimaging of mice. Ultrasound Med Biol 2002;28:1165–72.
[12] Behler RH, Nichols TC, Zhu H, Merricks EP, Gallippi CM. ARFI imaging for noninvasive material characterization of atherosclerosis part II: toward in vivo characterization. Ultrasound Med Biol 2009;35:278–95.
[13] Gessner RC, Aylward SR, Dayton PA. Mapping microvasculature with acoustic angiography yields quantifiable differences between healthy and tumor-bearing tissue volumes in a rodent model. Radiology 2012;264:733–40.
[14] Feingold S, Gessner R, Guracar IM, Dayton PA. Quantitative volumetric perfusion mapping of the microvasculature using contrast ultrasound. Invest Rad 2010;45:669–74.
[15] Wang Y, Cui C, Miguez P, Yamauchi M, Costello J, Wauthier E, et al. Lineage restriction of hepatic stem cells to mature fates is made efficient by tissue-specific biomatrix scaffolds. Hepatology 2011;53:293–305.
[16] Gessner R, Lukacs M, Lee M, Cherin E, Foster FS, Dayton PA. High-resolution, high-contrast ultrasound imaging using a prototype dual-frequency transducer: *in vitro* and *in vivo* studies. IEEE Trans Ultrason Ferroelectr Freq Control 2010;57:1772–81.
[17] Streeter JE, Herrera-Loeza SG, Neel NF, Yeh JJ, Dayton PA. A comparative evaluation of ultrasound perfusion imaging, molecular imaging, and volume measurements in evaluating the response to therapy. Tech Cancer Res Treat 2013;12:311–21.
[18] Reid LM, Fiorino AS, Sigal SH, Brill S, Holst PA. Extracellular matrix gradients in the space of Disse: relevance to liver biology. Hepatology 1992;15:1198–203.
[19] Knowles BB, Howe CC, Aden DP. Human hepatocellular carcinoma cell lines secrete the major plasma proteins and hepatitis B surface antigen. Science 1980;209:497–9.
[20] Darlington GJ, Kelly JH, Buffone GJ. Growth and hepatospecific gene expression of human hepatoma cells in a defined medium. In Vitro Cell Dev Biol 1987;23:349–54.
[21] Lindner JR, Song J, Jayaweera AR, Sklenar J, Kaul S. Microvascular rheology of definity microbubbles after intra-arterial and intravenous administration. J Am Soc Echocardiogr 2002;15:396–403.
[22] Wei K, Jayaweera AR, Firoozan S, Linka A, Skyba DM, Kaul S. Quantification of myocardial blood flow with ultrasound-induced destruction of microbubbles administered as a constant venous infusion. Circulation 1998;97:473–83.
[23] Kruse DE, Ferrara KW. A new imaging strategy using wideband transient response of ultrasound contrast agents. IEEE Trans Ultrason Ferroelectr Freq Control 2005;52:1320–409.
[24] Kogan P, Johnson KA, Feingold S, Garrett N, Guracar I, Arendshorst WJ, et al. Validation of dynamic contrast-enhanced ultrasound in rodent kidneys as an absolute quantitative method for measuring blood perfusion. Ultrasound Med Biol 2011;37:900–8.
[25] Badylak SF, Taylor D, Uygun K. Whole-organ tissue engineering: decellularization and recellularization of three-dimensional matrix scaffolds. Annu Rev Biomed Eng 2011;13:27–53.
[26] Baptista PM, Siddiqui MM, Lozier G, Rodriguez SR, Atala A, Soker S. The use of whole organ decellularization for the generation of a vascularized liver organoid. Hepatology 2011;53:604–17.
[27] Gupta S, Rajvanshi P, Sokhi R, Slehria S, Yam A, Kerr A, et al. Entry and integration of transplanted hepatocytes in rat liver plates occur by disruption of hepatic sinusoidal endothelium. Hepatology 1999;29:509–19.
[28] Malhi H, Irani A, Volenberg I, Schilsky ML, Gupta S. Early cell transplantation in LEC rats modeling Wilson's disease eliminates hepatic copper with reversal of liver disease. Gastroenterology 2002;122:438–47.
[29] Badylak S, Arnoczky S, Plouhar P, Haut R, Mendenhall V, Clarke R, et al. Naturally occurring extracellular matrix as a scaffold for musculoskeletal repair. Clin Orthop Relat Res 1999:S333–43.
[30] Badylak SF. The extracellular matrix as a scaffold for tissue reconstruction. Semin Cell Dev Biol 2002;13:377–83.
[31] Uygun B, Soto-Gutierrez A, Yagi H, Izamis M, Guzzardi MA, Shulman C, et al. Organ re-engineering through development of a transplantable recellularized liver graft using decellularized liver matrix. Nat Med 2010;16:814–20.
[32] Taylor DA, Atkins BZ, Hungspreugs P, Jones TR, Reedy MC, Hutcheson KA, et al. Regenerating functional myocardium: improved performance after skeletal myoblast transplantation. Nat Med 1998;4:929–33.
[33] Baptista PM, Orlando G, Mirmalek-Sani S, Siddiqui M, Atala A, Soker S. Whole organ decellularization-a tool for bioscaffold fabrication and organ bioengineering. Conf Proc IEEE Eng Med Biol Soc 2009:6526–9.